Journal of Zhejiang University SCIENCE A
ISSN 1673-565X (Print); ISSN 1862-1775 (Online)
www.zju.edu.cn/jzus; www.springerlink.com
E-mail: jzus@zju.edu.cn

A maximum a posteriori super resolution algorithm based on multidimensional Lorentzian distribution*

Wen CHEN†1, Xiang-zhong FANG[1], Yan CHENG[2]

([1]*Shanghai Key Lab of Digital Media Processing and Transmissions, Institute of Image Communication and Information Processing, Shanghai Jiao Tong University, Shanghai 200240, China*)

([2]*College of Information Technology, East China University of Political Science and Law, Shanghai 201620, China*)

†E-mail: chenwen_01@yahoo.com.cn

Received Jan. 6, 2009; Revision accepted Apr. 24, 2009; Crosschecked Oct. 18, 2009

Abstract: This paper presents a threshold-free maximum a posteriori (MAP) super resolution (SR) algorithm to reconstruct high resolution (HR) images with sharp edges. The joint distribution of directional edge images is modeled as a multidimensional Lorentzian (MDL) function and regarded as a new image prior. This model makes full use of gradient information to restrict the solution space and yields an edge-preserving SR algorithm. The Lorentzian parameters in the cost function are replaced with a tunable variable, and graduated nonconvexity (GNC) optimization is used to guarantee that the proposed multidimensional Lorentzian SR (MDLSR) algorithm converges to the global minimum. Simulation results show the effectiveness of the MDLSR algorithm as well as its superiority over conventional SR methods.

Key words: Edge preservation, Multidimensional Lorentzian distribution (MDL), Super resolution, Threshold
doi:10.1631/jzus.A0920013 **Document code:** A **CLC number:** TN911.73

INTRODUCTION

High resolution (HR) images are often required in medical, surveillance, forensic, satellite and other applications. In reality, however, the image resolutions are far from desired. The objective of a multiframe super resolution (SR) algorithm is to produce an HR image by combining multiple low resolution (LR) images.

The multiframe SR problem was first addressed by Tsai and Huang (1984), who proposed a frequency domain approach to restore an HR image from several noise-free LR images. This approach was extended to a blurred and noisy case by Kim *et al*.(1990). Although the frequency domain methods are very simple, they are restricted to global translational motion and linear space invariant (LSI) blur, which limits their use. An alternative SR approach reconstructs the HR image in the spatial domain. Irani and Peleg (1991) suggested the iterative backprojection (IBP) method, in which the HR image is estimated by back projecting the difference between the simulated LR images and the observed LR images. The main disadvantages of the IBP method are the non-unique solutions and the difficulty of applying a priori constraints. Another spatial domain SR method is projection onto convex sets (POCS), proposed by Stark and Oskoui (1989). This method can easily incorporate prior knowledge into the estimation process, but its solution is also non-unique and depends on the initial guess. A maximum likelihood (ML) SR method (Zhu *et al*., 2007) has also been presented. As it lacks a regularization term, this method is very sensitive to noise and the solution is still non-unique. One of the most promising SR approaches is the maximum a posteriori (MAP) estimator (Segall *et al*., 2004; Chantas *et al*., 2007), which uses a Bayesian framework for the inclusion of a priori constraints. When the prior term is convex, the MAP estimator ensures the existence

* Project (Nos. 60705012 and 60802025) supported by the National Natural Science Foundation of China

and uniqueness of the solution. Our work concentrates on the MAP SR algorithm.

A critical issue of MAP SR is the choice of a prior model for the desired HR image. In recent years, many image models have been presented. Schultz and Stevenson (1996) employed a Huber Markov random field (HMRF) model, which preserves edges while imposing smoothness constraints on the solution. This image model needs a threshold to distinguish edges and smooth regions. Such a threshold has to be tuned for every new case since it is dependent on image content and noise. In practical applications, however, it is not easy to determine the appropriate threshold. Hardie *et al*.(1997) presented a threshold-free Gaussian Markov random field (GMRF), which takes a quadratic form and penalizes the high-frequency components severely, resulting in a solution with excessively smoothed edges. Segall *et al*. (2004) used a simultaneously autoregressive (SAR) model for compressed videos. Such a model tends to produce blurred edges in the reconstructed image because it assumes that the statistics of the HR image are constant in different spatial locations. Donaldson and Myers (2005) proposed a text-specific bimodal prior model, which is inapplicable to general images. Chantas *et al*.(2007) introduced a hierarchical image model, where both the normalization constant and the hyper-parameters must be found heuristically, increasing the computational complexity. Recently, learning-based MAP SR methods have also been proposed, where the prior models are derived from collections of training samples (Baker and Kanade, 2002; Haber and Tenorio, 2003). Because of the need for a large number of examples, these methods are effective only when applied to specific scenarios, such as text or faces. The one-dimensional Lorentzian (1DL) function, usually serving as an error norm in robust SR algorithms (Patanaviji *et al*., 2007; El-Yamany and Papamichalis, 2008), has also been used as an image model. In non-linear image restoration algorithms for a passive millimeter-wave image (Lettington *et al*., 2001), the 1DL model was introduced as a correction term to reduce ringing artifacts. A similar approach was used in the single-frame Poisson MAP SR algorithm for 1D images (Lettington and Hong, 1995). In the multiframe SR algorithm proposed by Cheng *et al*.(2007), the 1DL model was used as a regularization term, yielding a threshold-free SR algorithm with edge preservation. Although its advantages over traditional image models are obvious, the 1DL model has a serious disadvantage when used in 2D multiframe SR algorithms: the solution may be non-unique as only the one-directional prior constraint is imposed.

In this paper, we extend the 1DL model and present a new multidimensional Lorentzian (MDL) image prior which uses gradient information in horizontal, vertical and diagonal directions to restrict the solution space. The proposed MDL model penalizes small gradients severely but penalizes large gradients less severely, resulting in an edge-preserving SR algorithm. In addition, the steepest descent algorithm adopted in the above 1DL methods may become trapped in local minima because the Lorentzian function is not convex over the entire domain, degrading the algorithm performance. In this paper, the Lorentzian parameters in the cost function are replaced with a tunable variable, and graduated non-convexity (GNC) optimization (Nielsen, 1997) is used to guarantee that the proposed multidimensional Lorentzian SR (MDLSR) algorithm converges to the global minimum.

MAXIMUM A POSTERIORI SUPER RESOLUTION FRAMEWORK

To formulate the algorithm, we first introduce the observation model, which reveals the relation between the original HR image and the observed LR images. An observation model can be described as in Eq.(1) with all vectors being ordered lexicographically (Park *et al*., 2003):

$$\boldsymbol{y}_k = \boldsymbol{W}_k \boldsymbol{x} + \boldsymbol{n}_k, \quad 1 \le k \le q, \tag{1}$$

where $\boldsymbol{y}_k$ is the kth observed LR image with the size of $N_1N_2\times1$; $\boldsymbol{x}$ is the $l_1l_2N_1N_2\times1$ HR image, and l_1 and l_2 are the horizontal and vertical downsampling factors, respectively; $\boldsymbol{n}_k$ is the additive noise vector in the kth LR image; degradation matrix $\boldsymbol{W}_k$ denotes warping, blurring and subsampling operations. A simple illustration for the observation model is given in Fig.1.

Because of insufficient LR images and ill-conditioned blur operators in Eq.(1), the SR algorithm is an ill-posed inverse problem. The MAP method can

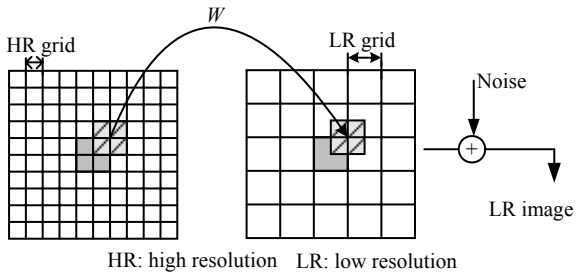

Fig.1 A simple illustration for the observation model

be applied to pick up a stable solution when the a posteriori probability density function (PDF) $P(\boldsymbol{x}|\boldsymbol{y}_1, \boldsymbol{y}_2, \ldots, \boldsymbol{y}_q)$ is available. The MAP estimator maximizes $P(\boldsymbol{x}|\boldsymbol{y}_1, \boldsymbol{y}_2, \ldots, \boldsymbol{y}_q)$ with respect to $\boldsymbol{x}$ (Schultz and Stevenson, 1996) as follows:

$$\hat{\boldsymbol{x}} = \arg\max_{\boldsymbol{x}} \{P(\boldsymbol{x} \mid \boldsymbol{y}_1, \boldsymbol{y}_2, \cdots, \boldsymbol{y}_q)\}. \tag{2}$$

Applying the Bayesian Theorem, we can obtain

$$\begin{aligned}\hat{\boldsymbol{x}} &= \arg\max_{\boldsymbol{x}} \left\{ \frac{P(\boldsymbol{y}_1, \boldsymbol{y}_2, \cdots, \boldsymbol{y}_q \mid \boldsymbol{x}) P(\boldsymbol{x})}{P(\boldsymbol{y}_1, \boldsymbol{y}_2, \cdots, \boldsymbol{y}_q)} \right\} \\ &= \arg\max_{\boldsymbol{x}} \{P(\boldsymbol{y}_1, \boldsymbol{y}_2, \cdots, \boldsymbol{y}_q \mid \boldsymbol{x}) P(\boldsymbol{x})\} \\ &= \arg\min_{\boldsymbol{x}} \{-\ln P(\boldsymbol{y}_1, \boldsymbol{y}_2, \cdots, \boldsymbol{y}_q \mid \boldsymbol{x}) - \ln P(\boldsymbol{x})\},\end{aligned} \tag{3}$$

where $P(\boldsymbol{y}_1, \boldsymbol{y}_2, \ldots, \boldsymbol{y}_q|\boldsymbol{x})$ denotes the noise distribution and $P(\boldsymbol{x})$ is the PDF of the HR image $\boldsymbol{x}$.

MULTIDIMENSIONAL LORENTZIAN SUPER RESOLUTION ALGORITHM

Multidimensional Lorentzian model

An appropriate choice of a priori model $P(\boldsymbol{x})$ is critical to MAP SR algorithm performance. Traditional image models either produce oversmoothed solutions or depend on threshold parameters. Recently, a threshold-free 1DL image model was introduced to multiframe SR (Cheng *et al*., 2007) which can obtain edge-preserving solutions. However, since only one-directional prior constraint is used, the solution of the resulting SR algorithm may be non-unique, degrading the algorithm's performance.

Here we present a new image model based on multi-directional edge images. We consider the first-order difference of a 2D image $\boldsymbol{x}$ for the pixel (j_1, j_2) in horizontal, vertical and diagonal directions,

$$\begin{cases} \varepsilon_1(j_1, j_2) = x(j_1+1, j_2) - x(j_1, j_2), \\ \varepsilon_2(j_1, j_2) = x(j_1+1, j_2+1) - x(j_1, j_2), \\ \varepsilon_3(j_1, j_2) = x(j_1, j_2+1) - x(j_1, j_2), \\ \varepsilon_4(j_1, j_2) = x(j_1-1, j_2+1) - x(j_1, j_2), \end{cases} \tag{4}$$

which can also be written as $\boldsymbol{Q}_i\boldsymbol{x}=\boldsymbol{\varepsilon}_i$ (i=1, 2, 3, 4), where $\boldsymbol{Q}_i$ is the directional difference operator and $\boldsymbol{\varepsilon}_i=[\varepsilon_{i,1}, \varepsilon_{i,2}, \cdots, \varepsilon_{i,l_1 l_2 N_1 N_2}]^{\mathrm{T}}$ is the ith edge image.

Fig.2 illustrates the edge images of the Lena image and the corresponding histograms. The histogram of each edge image usually has a sharper peak and a longer tail than the Gaussian function and can be described approximately as a Lorentzian distribution (Lettington *et al.*, 2001) as follows:

$$P(\boldsymbol{\varepsilon}_i) = \prod_{m=1}^{l_1 l_2 N_1 N_2} \frac{a_i / \pi}{\varepsilon_{i,m}^2 + a_i^2}, \quad 1 \le i \le 4, \tag{5}$$

where the Lorentzian parameter a_i is the half width at half maximum height of the distribution function, which characterizes the sharpness of the edge image, and $\varepsilon_{i,m}$ is the mth element of the vector $\boldsymbol{\varepsilon}_i$. a_i can be calculated using the following equation:

$$a_i = \frac{1}{\pi p_{i\max}}, \tag{6}$$

where $p_{i\max}$ is the histogram peak height of the ith edge image.

To make subsequent calculations tractable, edges are assumed to be independent. The joint density for four edge images is given by

$$P(\boldsymbol{\varepsilon}_1, \boldsymbol{\varepsilon}_2, \boldsymbol{\varepsilon}_3, \boldsymbol{\varepsilon}_4) = P(\boldsymbol{\varepsilon}_1) P(\boldsymbol{\varepsilon}_2) P(\boldsymbol{\varepsilon}_3) P(\boldsymbol{\varepsilon}_4). \tag{7}$$

Because $P(\boldsymbol{\varepsilon}_1, \boldsymbol{\varepsilon}_2, \boldsymbol{\varepsilon}_3, \boldsymbol{\varepsilon}_4)$ is the product of four 1D Lorentzian functions and contains four parameters a_i (i=1, 2, 3, 4), we use the term 'multidimensional Lorentzian distribution' to describe it. For a piecewise constant image with smoothness property, the intensity varies gradually over regions except in the vicinity of edges. We assume that a smooth image consists of edges and several known base values. Therefore, minimizing the negative logarithm likelihood of the original image is equivalent to minimizing that of the edge images.

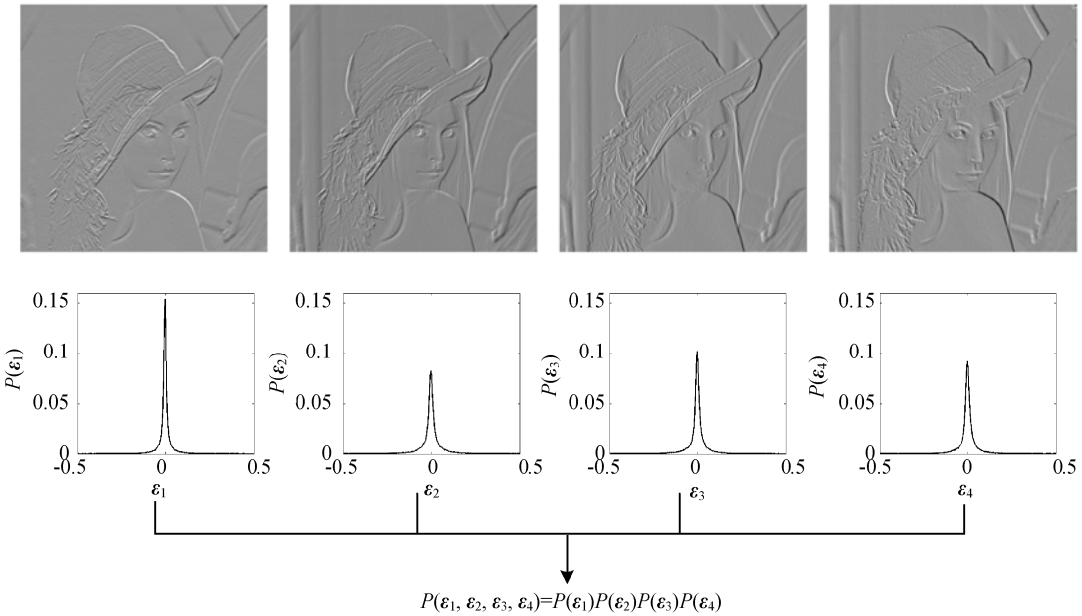

Fig.2 Edge images of Lena and the corresponding histograms

Suppose that noise in each LR image follows independent and identically distributed (i.i.d.) Gaussian distributions with zero means and variances σ_n^2. We have

$$P(\boldsymbol{y}_1, \boldsymbol{y}_2, \cdots, \boldsymbol{y}_q \mid \boldsymbol{x}) = \prod_{k=1}^{q} P(\boldsymbol{y}_k \mid \boldsymbol{x}) = \frac{1}{(2\pi\sigma_n^2)^{qN_1N_2/2}} \exp\left(-\sum_{k=1}^{q} \frac{\| \boldsymbol{y}_k - \boldsymbol{W}_k \boldsymbol{x} \|^2}{2\sigma_n^2} \right), \tag{8}$$

where $\|\cdot\|$ stands for the Euclidean distance. Combining Eqs.(3), (5) and (8), the optimization expression can be written as

$$\hat{\boldsymbol{x}} = \arg\min_{\boldsymbol{x}} J(\boldsymbol{x}), \tag{9}$$

$$\begin{aligned} J(\boldsymbol{x}) &= -\ln\{P(\boldsymbol{y}_1, \boldsymbol{y}_2, \cdots, \boldsymbol{y}_q \mid \boldsymbol{x})\} - \lambda \ln\{P(\boldsymbol{x})\} \\ &= \sum_{k=1}^{q} \| \boldsymbol{y}_k - \boldsymbol{W}_k \boldsymbol{x} \|^2 - \lambda \sum_{i=1}^{4} \sum_{m=1}^{l_1 l_2 N_1 N_2} \ln\left(\frac{a_i / \pi}{\varepsilon_{i,m}^2 + a_i^2} \right) \\ &= \sum_{k=1}^{q} \| \boldsymbol{y}_k - \boldsymbol{W}_k \boldsymbol{x} \|^2 + \lambda \sum_{m=1}^{l_1 l_2 N_1 N_2} \left[\sum_{i=1}^{4} \ln\left(1 + \frac{\varepsilon_{i,m}^2}{a_i^2} \right) \right] \\ &\quad + \lambda \sum_{m=1}^{l_1 l_2 N_1 N_2} \sum_{i=1}^{4} \ln(a_i \pi), \end{aligned} \tag{10}$$

where $J(\boldsymbol{x})$ is the cost function and λ is the regularization parameter.

Because the last term in the right-hand side of Eq.(10) is irrelative to $\boldsymbol{x}$, it can be omitted from the optimization process.

Modification and implementation

Because the first term of $J(\boldsymbol{x})$ is a convex function, the convexity of the cost function is dependent on the second term. The function $z(\varepsilon)=\ln(1+\varepsilon^2/a^2)$ is convex in the band $B=(-a, a)$ (Fig.3). Hence, the second term of $J(\boldsymbol{x})$ is convex in the band $(-a_{\min}, a_{\min})$, where $a_{\min}=\min\{a_1, a_2, a_3, a_4\}$. That is, the convexity of the cost function is determined by four parameters a_i (i=1, 2, 3, 4), resulting in a computationally complex optimization process. To make the problem more tractable, we slightly modify the logarithm prior as

$$L(\boldsymbol{\varepsilon}) = \sum_{m=1}^{l_1 l_2 N_1 N_2} \left[\sum_{i=1}^{4} \ln\left(1 + \frac{\varepsilon_{i,m}^2}{\tau^2} \right) \right], \tag{11}$$

where the Lorentzian parameters a_i are replaced by a global variable τ. The value of τ controls the shape of $L(\boldsymbol{\varepsilon})$. A large value of τ makes Eq.(11) convex. Then $J(\boldsymbol{x})$ can be rewritten as follows:

$$J(\boldsymbol{x}) = \sum_{k=1}^{q} \| \boldsymbol{y}_k - \boldsymbol{W}_k \boldsymbol{x} \|^2 + \lambda \sum_{m=1}^{l_1 l_2 N_1 N_2} \left[\sum_{i=1}^{4} \ln\left(1 + \frac{\varepsilon_{i,m}^2}{\tau^2} \right) \right]. \tag{12}$$

The gradient of $J(\boldsymbol{x})$ at the nth iteration is calculated using the following equation:

$$\nabla J(\boldsymbol{x}^n)=2\sum_{k=1}^{q}\boldsymbol{W}_k^{\mathrm{T}}(\boldsymbol{W}_k\boldsymbol{x}^n-\boldsymbol{y}_k)+\lambda\nabla G^{(n)}, \quad (13)$$

where $\nabla G^{(n)}$ is the first derivative of the second term of Eq.(12).

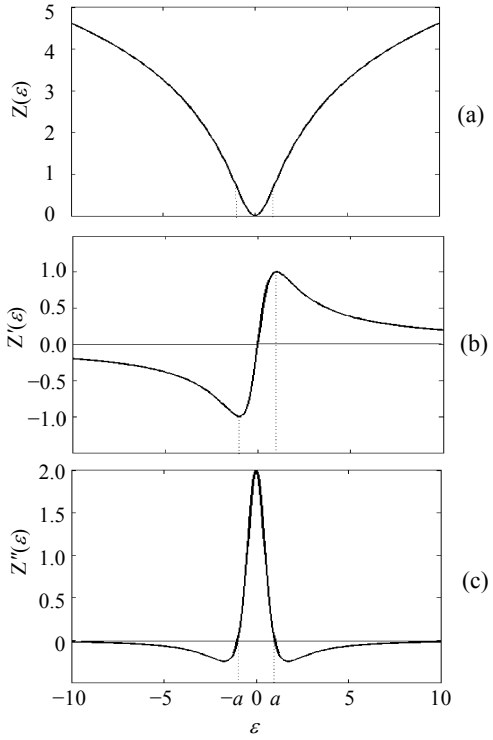

Fig.3 The curves of (a) $z(\varepsilon)=\ln(1+\varepsilon^2/a^2)$, (b) the first derivative of $z(\varepsilon)$, and (c) the second derivative of $z(\varepsilon)$

From Fig.3b, the absolute value of the first derivative of $z(\varepsilon)$ increases rapidly up to a point and starts to decrease as the magnitude of the gradient grows. Because of this property, the cost function penalizes small gradients severely but penalizes large gradients less severely. Usually, a small gradient is caused by noise while a large gradient value corresponds to an edge. Hence, the proposed MDL model yields an edge-preserving algorithm.

Because the cost function $J(\boldsymbol{x})$ is not convex over the entire domain, a simple gradient descent method, as adopted by previous 1DL methods, may become trapped in local minima. To ensure that the proposed MDLSR algorithm converges to the global minimum, in this work, we use the graduated nonconvexity (GNC) optimization approach. Firstly, a large value of τ is chosen to guarantee the strict convexity of $J(\boldsymbol{x})$ and a gradient descent algorithm is used to find the unique minimum. This minimum is then used as the initial value for the next phase of optimization with a smaller τ. The above two steps are repeated until the algorithm converges. Note that the initial value of τ must be large enough to avoid the problem of local minima. By gradually decreasing τ to a low value, the edges are preserved in the final solution. The steps of the proposed algorithm are described in Table 1.

Table 1 The proposed MDLSR algorithm

Step 1: Choose a reference LR image, and bilinearly interpolate it to obtain an initial estimate $\boldsymbol{x}^0$.
Step 2: Compute the four edge images $\boldsymbol{\varepsilon}_i^0$ (i=1, 2, 3, 4) of $\boldsymbol{x}^0$, and estimate their respective Lorentzian parameters a_i using Eq.(6).
Step 3: Choose $\tau^0=2\times\min\{a_1, a_2, a_3, a_4\}$, where the weight 2 is used to ensure that this initial global variable is large enough.
Step 4: n=0.
Step 5: Do {
1. Compute the gradient $\nabla J(\boldsymbol{x}^n)$ using Eq.(13);
2. Update $\boldsymbol{x}^n$ according to $\boldsymbol{x}^{n+1}=\boldsymbol{x}^n-\beta\cdot\nabla J(\boldsymbol{x}^n)$;
3. Set $n=n+1$;
4. If ($\|\boldsymbol{x}^n-\boldsymbol{x}^{n+1}\|<\delta$)
set $\tau^n=\max\{k\tau^{n-1}, \tau_{\text{target}}\}$;
} While ($\tau^n!=\tau_{\text{target}}$ OR $\|\boldsymbol{x}^n-\boldsymbol{x}^{n+1}\|>\delta$)
Step 6: Set the final solution $\hat{\boldsymbol{x}}=\boldsymbol{x}^n$.

$\boldsymbol{x}^0$: the initial estimate; $\boldsymbol{x}^n$: the partially reconstructed HR image; τ^n: the Lorentzian parameter in the nth iteration; τ_{target}: the target value of τ; k: the scale factor with which τ^n decreases slowly toward τ_{target}; β: the step size; δ: the constant for testing the convergence

EXPERIMENTAL RESULTS

In this section, we describe the results of tests on the performance of the proposed MDLSR algorithm on both synthetic and real data. In the synthetic experiments, the LR sequences were created in four cases listed in Table 2 by warping, blurring, downsampling and adding Gaussian noise to the Bill image (128×128 pixels) and Foreman image (176×144 pixels). In each case, the global motion vectors ($\boldsymbol{S}^{\mathrm{T}}$) can be represented by the Cartesian product of horizontal and vertical motion components. For instance, $\boldsymbol{S}^{\mathrm{T}}=\{0,1\}\times\{0,1\}=\{(0,0), (0,1), (1,0), (1,1)\}$. σ_{B}^2 represents the variance of the blurring kernel.

Table 2 Four cases of the synthesis experiments

Case	$\boldsymbol{S}^T$ of the HR image	Blurring	Downsampling factor
1	{0,0.5}×{0,0.5}	3×3 (σ_B^2=1)	2
2	{0,1}×{0,1}	3×3 (σ_B^2=2)	2
3	{0,1}×{0,1}	5×5 (σ_B^2=3)	2
4	{0,1,2}×{0,1,2}	3×3 (σ_B^2=1)	3

The reconstructed images were estimated from the synthetic LR images by applying the MDLSR algorithm. We also compared the proposed algorithm with GMRF (Hardie *et al*., 1997), HMRF (Schultz and Stevenson, 1996), and Lorentzian-based MAP (LBMAP) (Cheng *et al*., 2007). The parameter settings for the proposed algorithm were as follows: β=0.1, δ=0.005, τ_{target}=1 and k=0.9, which yielded the best visual qualities. The peak signal-to-noise ratio (PSNR) was used for quantitative evaluation:

$$\text{PSNR}=10\lg\frac{l_1 l_2 N_1 N_2\times 255^2}{\|\boldsymbol{x}-\hat{\boldsymbol{x}}\|^2}, \tag{14}$$

where $\boldsymbol{x}$ is the original image and $\hat{\boldsymbol{x}}$ is the reconstructed image.

To analyze the performance of different algorithms, we compared the PSNR in the case of different noise variances (σ_n^2). Figs.4 and 5 are the plots of PSNR versus σ_n^2 for the Bill and Foreman images. It can be seen that the performance of GMRF was the worst among these methods. HMRF was much better than GMRF, but its performance was dependent on the threshold parameter T. For both the Bill and Foreman images, the performance with T=1 was better than that with T=3. The PSNR values of LBMAP were slightly poorer than those of HMRF (T=1), because of insufficient prior information and because the simple steepest descent optimization was used to reconstruct the HR image, which might have degraded the performance of LBMAP. As expected, the proposed MDLSR algorithm performed the best among these algorithms, especially in the cases of low noise variances.

Figs.6 and 7 provide the visual comparison of the algorithms for the Bill image of case 1 with σ_n^2=10 and the Foreman image of case 4 with σ_n^2=40, respectively. From Fig.6, the reconstructed image of GMRF was oversmoothed. The edges were somewhat blurry in the reconstructed image of LBMAP. Although the PSNR value of HMRF (T=1) was higher than that of LBMAP (by about 0.2 dB on average), the visual improvement was not obvious. In comparison with these algorithms, our MDLSR algorithm not only preserved the edges effectively, but also suppressed noise very well. Similar results can be found for the Foreman image (Fig.7).

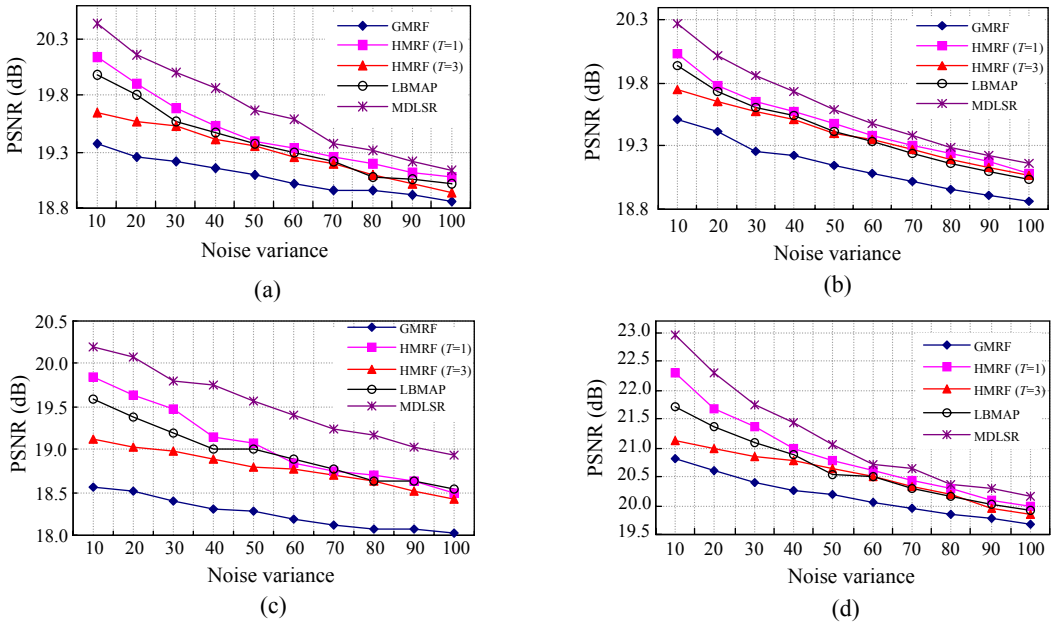

Fig.4 Plots of PSNR versus σ_n^2 for the Bill image: (a) Case 1; (b) Case 2; (c) Case 3; (d) Case 4

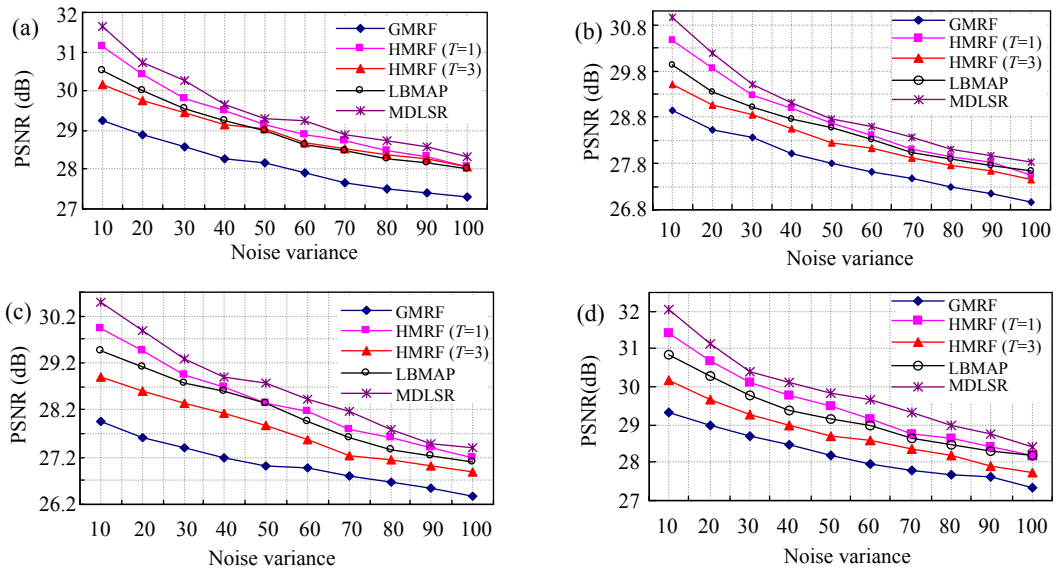

Fig.5 Plots of PSNR versus σ_n^2 for the Foreman image: (a) Case 1; (b) Case 2; (c) Case 3; (d) Case 4

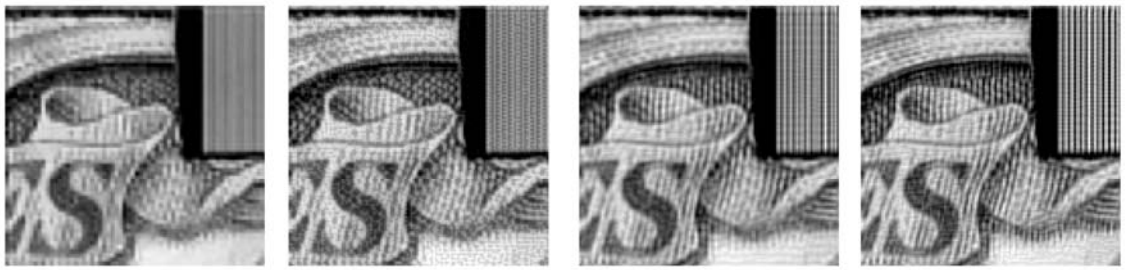

(a) (b) (c) (d)

Fig.6 Reconstructed images of the Bill image

(a) GMRF (19.38 dB); (b) HMRF (T=1) (20.14 dB); (c) LBMAP (19.99 dB); (d) MDLSR (20.45 dB)

(a) (b) (c) (d)

Fig.7 Reconstructed images of the Foreman image

(a) GMRF (28.47 dB); (b) HMRF (T=1) (29.76 dB); (c) LBMAP (29.40 dB); (d) MDLSR (30.12 dB)

Our third experiment was a real sequence of 8 LR Bookcase images of size 176×144. Fig.8a shows one of the LR images. The unknown point spread function (PSF) was assumed to be a 3×3 Gaussian kernel with a standard deviation equal to 1. We used the method of Suh and Jeong (2004) to estimate the motion parameters. A threshold value of 2 was chosen for HMRF as it yielded the best visual quality. The reconstructed HR images enhanced by a factor of 2 are shown in Figs.8b~8e. Fig.9 shows small portions of them for ease of comparison. The result of GMRF was quite blurred, and most of the texts were not at all readable. HMRF performed better than GMRF, but some texts were not easily discernible. The subjective performance of LBMAP was close to that of HMRF. In comparison, the proposed MDLSR algorithm gave the best reconstructed image with sharp edges. The readability of the texts was significantly improved.

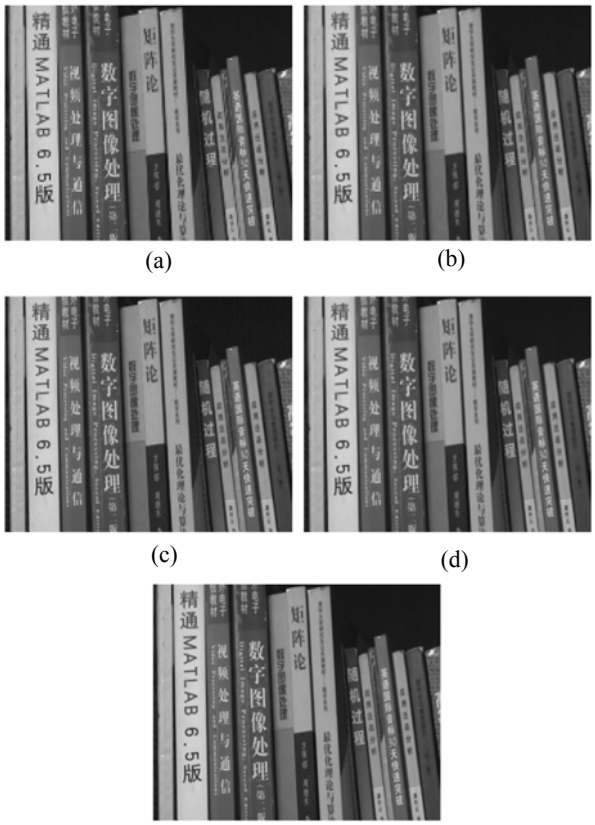

(a) (b) (c) (d) (e)

Fig.8 (a) One of the LR images; Reconstructed HR images of (b) GMRF, (c) HMRF, (d) LBMAP, and (e) MDLSR

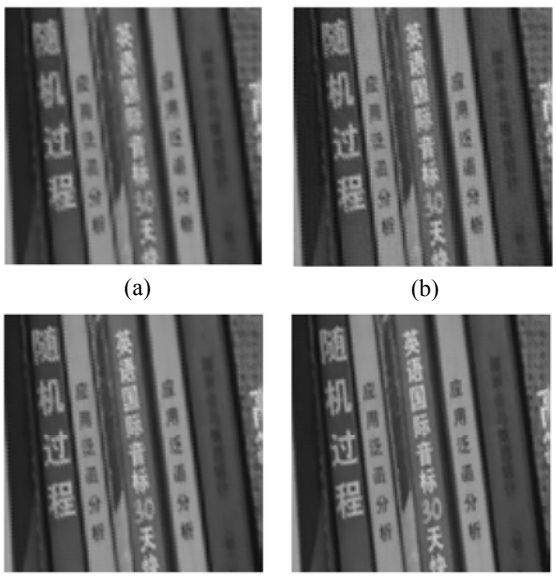

(a) (b) (c) (d)

Fig.9 Sections taken from the reconstructed images of (a) GMRF, (b) HMRF, (c) LBMAP, and (d) MDLSR

CONCLUSION

In this paper, a new image model of multidimensional Lorentzian distribution is proposed for the MAP multiframe SR algorithm. The proposed model combines the statistic characteristics of the directional edge images to impose sufficient constraints on the solution space and yields an edge-preserving SR algorithm. The Lorentzian parameters in the cost function are replaced with a tunable global variable, and GNC optimization is adopted to guarantee the convergence of the SR algorithm to the global minimum. The effectiveness of the proposed MDLSR algorithm was demonstrated using synthetic and real data. Simulation results clearly indicated that the proposed algorithm obtains higher PSNR values and sharper edges compared with conventional methods.

References

Baker, S., Kanade, T., 2002. Limits on super-resolution and how to break them. *IEEE Trans. Pattern Anal. Mach. Intell.*, **24**(9):1167-1183. [doi:10.1109/TPAMI.2002.1033210]

Chantas, G.K., Galatsanos, N.P., Woods, N.A., 2007. Super-resolution based on fast registration and maximum a posteriori reconstruction. *IEEE Trans. Image Process.*, **16**(7):1821-1830. [doi:10.1109/TIP.2007.896664]

Cheng, Y., Fang, X.Z., Yang, X.K., 2007. Edge-image-based approach for stable super-resolution reconstruction. *Opt. Eng.*, **46**(2):027004. [doi:10.1117/1.2697902]

Donaldson, K., Myers, G.K., 2005. Bayesian super-resolution of text in video with a text-specific bimodal prior. *Int. J. Docum. Anal. Recogn.*, **7**(2-3):159-167. [doi:10.1007/s10032-004-0139-y]

El-Yamany, N.A., Papamichalis, P.E., 2008. Robust color image super-resolution: an adaptive M-estimation framework. *EURASIP J. Image Video Process.*, **2008**(2):38052. [doi:10.1155/2008/763254]

Haber, E., Tenorio, L., 2003. Learning regularization functionals: a supervised training approach. *Inv. Probl.*, **19**(3):611-626. [doi:10.1088/0266-5611/19/3/309]

Hardie, R.C., Barnard, K.J., Armstrong, E.E., 1997. Joint MAP registration and high-resolution image estimation using a sequence of undersampled images. *IEEE Trans. Image Process.*, **6**(12):1621-1633. [doi:10.1109/83.650116]

Irani, M., Peleg, S., 1991. Improving resolution by image registration. *CVGIP: Graph. Models Image Process.*, **53**(3):231-239. [doi:10.1016/1049-9652(91)90045-L]

Kim, S.P., Bose, N.K., Valenzuela, H.M., 1990. Recursive reconstruction of high resolution image from noisy undersampled multiframes. *IEEE Trans. Acoust., Speech, Signal Process.*, **38**(6):1013-1027. [doi:10.1109/29.56062]

Lettington, A.H., Hong, Q.H., 1995. Ringing artifact reduction for Poisson MAP superresolution algorithms. *IEEE Signal Process. Lett.*, **2**(5):83-84. [doi:10.1109/97.386284]

Lettington, A.H., Tzimopoulou, S., Rollason, M.P., 2001. Nonuniformity correction and restoration of passive millimeter-wave images. *Opt. Eng.*, **40**(2):268-274. [doi:10.1117/1.1339875]

Nielsen, M., 1997. Graduated nonconvexity by functional focusing. *IEEE Trans. Pattern Anal. Mach. Intell.*, **19**(5):521-525. [doi:10.1109/34.589213]

Park, S.C., Park, M.K., Kang, M.G., 2003. Super-resolution image reconstruction: a technical overview. *IEEE Signal Process. Mag.*, **20**(3):21-36. [doi:10.1109/MSP.2003.1203207]

Patanaviji, V., Tae-O-Sot, S., Jitapunkul, S., 2007. A Robust Iterative Super-resolution Reconstruction of Image Sequences Using a Lorentzian Bayesian Approach with Fast Affine Block-based Registration. IEEE Int. Conf. on Image Processing, p.393-396. [doi:10.1109/ICIP.2007.4379848]

Schultz, R.R., Stevenson, R.L., 1996. Extraction of high-resolution frames from video sequences. *IEEE Trans. Image Process.*, **5**(6):996-1011. [doi:10.1109/83.503915]

Segall, C.A., Katsaggelos, A.K., Molina, R., Mateos, J., 2004. Bayesian resolution enhancement of compressed video. *IEEE Trans. Image Process.*, **13**(7):898-911. [doi:10.1109/TIP.2004.827230]

Stark, H., Oskoui, P., 1989. High resolution image recovery from image-plane arrays, using convex projections. *J. Opt. Soc. Am. A*, **6**(11):1715-1726. [doi:10.1364/JOSAA.6.001715]

Suh, J.W., Jeong, J., 2004. Fast sub-pixel motion estimation techniques having lower computational complexity. *IEEE Trans. Consum. Electron.*, **50**(3):968-973. [doi:10.1109/TCE.2004.1341708]

Tsai, R.Y., Huang, T.S., 1984. Multi-frame image restoration and registration. *Adv. Comput. Vis. Image Process.*, **1**(2):317-339.

Zhu, H., Lu, Y., Wu, Q., 2007. Super-resolution Image Restoration by Maximum Likelihood Method and Edge-oriented Diffusion. SPIE, **6625:**66250Y-1-8. [doi:10.1117/12.791021]